# Do Montmorillonite Surfaces Promote Methane Hydrate Formation? Monte Carlo and Molecular Dynamics Simulations

### Sung-Ho Park* and Garrison Sposito

*Geochemistry Department, Earth Sciences Division, Lawrence Berkeley National Laboratory, Berkeley, California 94720*

*Received: June 13, 2002*

Recent laboratory experiments on methane hydrate formation in the presence of Na-montmorillonite, a clay mineral found coexistently with hydrates in oceanic sediments, suggest that clay surfaces may facilitate methane hydrate crystallization from aqueous solution. Monte Carlo and molecular dynamics simulations were carried out to determine whether stable methane clathrates could in principle form in the interlayers of hydrated Na-montmorillonite in equilibrium with seawater under ambient conditions. Stable interlayer methane clathrate structures were indeed found to occur under pressures as low as 10 atm and at temperatures as high as 300 K in simulations of a three-layer hydrate of Na-montmorillonite containing 0.5 $CH_4$ per clay mineral unit cell. This result is consistent with a "thermodynamic promotion effect" of clay mineral surfaces on hydrate formation. Visualization of local methane clathrate structure in the 0.5 $CH_4$ per unit cell system revealed that the methane molecule is nested on a hexagonal ring of clay surface oxygens while surrounded by a clathrate-like water structure. The calculated $CH_4$−O coordination number was 20−22, in agreement with previous simulations and with neutron diffraction data on methane hydrate formation in bulk solution. Our MD simulations indicated that the power spectrum of the interlayer hydrate was essentially the same as that for the hydrate in bulk water. Higher methane loading than 0.5 $CH_4$ per unit cell was found to destabilize the hydrate structure similarly to a temperature increase. On the basis of these simulations, methane hydrate is proposed to occur in natural sediments with a portion of a clay mineral surface actively involved in promoting clathrate formation.

## 1. Introduction

Gas hydrates are nonstoichiometric crystalline compounds composed of small gas molecules (guests) and a vicinal cage-like water structure (the host).[1,2] Although there is no chemical bonding between the host water molecules and the enclosed guest molecule, van der Waals interactions lower the Gibbs energy of the water molecules, causing the clathrate to be stable.[3,4] Natural gas hydrates are abundant, most of them occurring just below the sea floor.[5] Oceanic methane hydrates, the most common form of natural clathrate,[6] have a biogenic origin and are found in sediments under certain concentration, pressure, and temperature conditions.[7] They have been considered as future energy resources because of the large amounts of hydrocarbon they store, but development has been retarded because of poor understanding of the thermodynamics and kinetics of their formation.[8]

Methane hydrate sI forms with two cavity sizes, pentagonal dodecahedron ($5^{12}$) and tetrakidecahedron ($5^{12}6^2$),[9] having methane−oxygen (water) coordination numbers of 20 and 24, respectively: Suitable pressure and temperature conditions for methane hydrate sI formation are found over most of the ocean floor, although formation normally is confined to continental margins where adequate supplies of gas are available.[10,11] The presence of methane under conditions within the pressure−temperature stability field for natural hydrates, however, is not sufficient to ensure hydrate formation. This occurs only when the mass fraction of dissolved methane exceeds its solubility in seawater and the methane flux exceeds a critical value corresponding to the rate of diffusive methane transport.[12] The growth
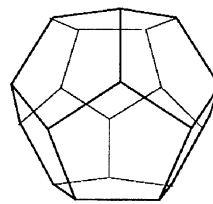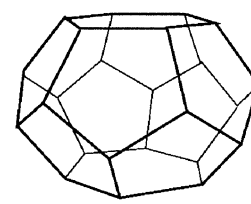


$5^{12}$        $5^{12}6^2$

rate and spatial distribution of gas hydrates in sediments have been quantified by mathematical models for hydrate formation in porous media.[13] Within the hydrate stability zone, the solubility of gas is largely controlled by temperature and decreases sharply toward the seafloor.[4]

The existence of the 2:1 clay mineral, smectite,[14] in marine environments is well-established,[15] and these minerals also are major components of the sediments where methane hydrates occur.[16] The iron-bearing smectite, nontronite,[14] widespread in oceanic sediments, has been considered as a possible fingerprint for naturally occurring methane hydrates.[17] Recent analyses of gas-hydrate-bearing marine sediments using neutron probes show that smectite is the most abundant mineral where the greatest gas hydrate saturation is found.[18] These minerals have a large interlayer surface on which loosely held hydrated cations reside.[14] Their crystal size varies from 0.2 to 2 $\mu$m, with an average size of 500 nm.[14,19]

There have been only a few studies dealing directly with the effect of 2:1 clay minerals on methane hydrate formation.[20−22] These experiments were performed typically with bentonite,

which is mainly Na-montmorillonite. Cha et al.[20] observed the dissociation of methane hydrate at higher temperature (296.1 K) and lower pressure (54.67 atm) in the presence of bentonite than observed for the same process in water alone (e.g., 295.7 K and 81.72 atm). They interpreted this thermodynamic P/T effect by hypothesizing that adsorbed water molecules on a clay mineral surface combine synergistically with methane to form the hydrate more easily. Ouar et al.[21] obtained similar results from experiments using bentonite drilling fluids with a methane-containing gas sample (87.2% methane). They observed hydrate formation at pressures as low as 54.4 atm and at temperatures as high as 294 K, thus confirming the experiments of Cha et al.[20] in observing unusual P/T conditions. They termed their result "thermodynamic promotion", but were unable to quantify the conditions for this promotion. Kotkoskie et al.[22] investigated 16 drilling muds and test fluids to ascertain their effect on methane hydrate P/T equilibrium conditions. They observed a hydrate to form at only 27 atm pressure and at 290 K, concluding that bentonite indeed has a promotion effect on hydrate formation. However, they also noted that the dissolved electrolyte (e.g., 20% NaCl) can inhibit hydrate formation by requiring higher pressure and lower temperature for P/T equilibrium than in pure water. They concluded that the net effect of bentonite in saline water is to promote hydrate formation.

Hydrate stability has been hypothesized also to be inhibited by the water adsorbed in fine-grained, clay-rich sediments because of the reduction of water activity in nanometer-sized pores,[16] particularly when the gas saturation is high. (Capillary effects and the electrical double layer of 2:1 clay minerals are the cause of low water activity in their interlayer regions.[23]) Buffett and Zatsepina[24] reported hydrate formation by dissolved $CO_2$ in Lane Mountain sand which they used in order to isolate aqueous solution from the gas phase. They observed dissolved $CO_2$ gas forming a hydrate at 20 atm pressure after diffusion into the porous medium with cooling from 290 K. They suggested that gas hydrates—including methane hydrates—should form and grow from dissolved methane in fluids contacting porous media and that the concentration of gas required to form a hydrate in the sea floor could be significantly lower than the concentration needed to form gas bubbles. Their experiments differed from those of Cha et al.[20] in showing that the hydrate can form in natural porous media even when free gas is absent. Thus, sediments may have an important role in hydrate formation and stability by providing nucleation sites and by altering the thermodynamic P/T conditions for stability.

Water ordering around methane during hydrate crystallization from aqueous solutions of methane over the temperature range 4−8 °C and at pressures of 34 and 145 atm has been investigated experimentally in the laboratory by isotopic substitution neutron diffraction.[25] A methane−water coordination number of 16 ± 1 in solution and 21 ± 1 in the hydrate was determined. Molecular dynamics simulations also have been used to investigate mechanisms of methane clathrate formation.[26,27] In these simulations, the host water structure began to relax after <1 ps. The host water cage thus was deemed unstable, rather than metastable, but with the guest molecules believed to contribute to the stability of the hydrate through repulsive forces.[27] Alteration of the behavior of the host water structure and its important role in stabilizing gas hydrates in the bulk were attributed wholly to the excluded volume of the guest molecules.[26]

Methane behavior in hydrated smectite interlayers recently was simulated by Titiloye and Skipper,[28] who used both Monte Carlo and molecular dynamics methods to determine the structure and mobility of methane in the interlayer region of Na-montmorillonite containing two layers of water. They used the TIP4P model of water for both constant stress (NσT) Monte Carlo and constant volume (NVT) molecular dynamics simulations. Their simulation cell comprised two molecular layers of water (64 water molecules), six sodium cations, and four methane molecules within opposing Wyoming-type smectite clay mineral layers. The P/T values studied were 260 K/1 bar (low-temperature regime), 280 K/1 bar (nominal 0 km burial depth), 310 K/150 bar, 325 K/225 bar, and 340 K/300 bar, the last conditions being those in a petroleum-rich sedimentary basin up to 2 km in depth. From MC simulation they observed a stable methane hydrate interlayer complex under the imposed P/T conditions. Besides methane solvation by 12−13 water molecules, six oxygen atoms from the clay surface were involved in completing the coordination shell. From MD simulation, they calculated methane self-diffusion coefficients, which ranged from 0.17 to $1.20 \times 10^{-9}$ m²/s, well-below the methane self-diffusion coefficient in pure water, $1.49 \times 10^{-9}$ m²/s.[29] The diffusion of interlayer species was attributed to a complex interplay between their hydrophobic and hydrophilic hydration.

Titiloye and Skipper[28] modeled the methane-water structure in Na-montmorillonite by varying pressure and temperature according to burial depth. However, they did not consider methane clathrate formation at low pressures (<50 atm) or at ambient temperature (300 K) where the promotional effect of 2:1 clay minerals on hydrate formation has been observed.[20−22] Thus, the "thermodynamic promotion effect" of clay surfaces has not yet been investigated by simulation under the P/T conditions at which it is observed.[20−22] In the present paper, we extend the study of Titiloye and Skipper[28] by elucidating the role of smectite interlayers in methane clathrate formation at the low pressures and ambient temperature conditions under which smectite has been reported to show a catalytic influence.[20−22] We approached our objective in a series of Monte Carlo simulations of a three-layer hydrate of Na-montmorillonite in equilibrium with seawater and with differing interlayer concentrations of methane under differing P/T conditions. Then we performed MD simulations on the MC-equilibrated hydrates to investigate interlayer species mobility and hydrate stability.

## 2. Methods

**2.1. Intermolecular Potential.** The model potential function used to represent intermolecular interactions is written:

$$U_{ij} = \sum_{i=1}^{N}\sum_{j \neq i}^{N} \frac{q_i q_j}{r_{ij}} - A_{ij}e^{-B_{ij}r_{ij}} + C_{ij}e^{-D_{ij}r_{ij}} \tag{1}$$

where $N$ is the total number of charge sites on atoms or molecules, $q_i$ is the effective charge of site $i$, and $r_{ij}$ is the inter-site distance. The effective charges $q$ for sites on water molecules and on atoms in the clay layer, and the van der Waals parameters ($A$, $B$, $C$, and $D$) describing short-range interactions between atoms in the water-cation-clay system are listed in Tables 1 and 2, respectively.

A four-point parameter adaptation to eq 1 was applied to the van der Waals interactions for methane−methane and methane−oxygen based on available Lennard-Jones 6-12 potentials:[30]

$$U_{LJ}(r) = \epsilon\left[\left(\frac{r_m}{r}\right)^{12} - 2\left(\frac{r_m}{r}\right)^{6}\right] \tag{2}$$

where $\epsilon = 0.2137$ and 0.2940 kcal mol$^{-1}$, and $r_m = 3.849$ and

Promoting Methane Hydrate Formation

*J. Phys. Chem. B, Vol. 107, No. 10, 2003* **2283**

**TABLE 1: Effective-Charge Parameters Used in Eq 1**

| atom | $q$(e) | atom | $q$ (e) |
|---|---|---|---|
| O ($T_d$ apical)[a] | $-1.0$ | (O)H (water) | 0.71748 |
| O (surface) | $-0.8$ | Si ($T_d$) | 1.2 |
| O(H) (clay) | $-1.7175$ | Al ($T_d$) | 0.2 |
| O(H) (water) | $-1.43496$ | Al ($O_h$)[b] | 3.0 |
| (O)H (clay) | 0.7175 | Mg($O_h$) | 2.0 |

[a] O ($T_d$ apical) denotes oxygen at the apex of a Si$-$O tetrahedron which also is part of the aluminum octahedral sheet. [b] Al ($O_h$) denotes the aluminum in the octahedral sheet.

**TABLE 2: van der Waals Interaction Parameters Used in Eq 1**

| sites | $A_{ij}$ (kcal mol$^{-1}$) | $B_{ij}$ (Å$^{-1}$) | $C_{ij}$ (kcal mol$^{-1}$) | $D_{ij}$ (Å$^{-1}$) |
|---|---|---|---|---|
| Water$-$Water | | | | |
| H$-$H | 0.0 | 0.0 | 666.33 | 2.7608 |
| H$-$O | 273.59 | 2.2333 | 1455.4 | 2.9619 |
| O$-$O | 0.0 | 0.0 | 1088213 | 5.1527 |
| Water-Clay | | | | |
| H$-$Si | 2.137 | 1.22 | 577.23 | 2.15646 |
| H$-$Al | 2.137 | 1.22 | 577.23 | 2.15646 |
| O$-$Si | 1345.8 | 2.2671 | 13061 | 3.2037 |
| O$-$Al | 1345.8 | 2.2671 | 13061 | 3.2037 |
| Water$-$Na$^+$ | | | | |
| H$-$Na | 884.2297 | 1.923886 | 2051.8654 | 2.3609517 |
| O$-$Na | 25.948129 | 0.77461042 | 61888.035 | 4.0849070 |
| Cation-Clay | | | | |
| Si$-$Na | 1505.4412 | 1.86517 | 2164.45 | 2.120855 |
| Al$-$Na | 1505.4412 | 1.86517 | 2164.45 | 2.120855 |
| CH$_4-$Water | | | | |
| O$-$CH$_4$ | 20.5880 | 1.11068 | 1499460.943 | 4.37568 |
| H$-$CH$_4$ | 0.0 | 0.0 | 0.0 | 0.0 |
| CH$_4-$CH$_4$ | | | | |
| CH$_4-$CH$_4$ | 28.3216 | 1.02102 | 2062716.29 | 4.02245 |

4.187 Å for CH$_4-$O and CH$_4-$CH$_4$, respectively. The corresponding potential from eq 1 is

$$U(r) = Ce^{-Dr} - Ae^{-Dr} \tag{3}$$

with the definitions

$$C \equiv \frac{\beta}{\delta - \beta}e^{\delta}\epsilon, \quad D \equiv \frac{\delta}{r_m}$$

$$A \equiv \frac{\delta}{\delta - \beta}e^{\beta}\epsilon, \quad B \equiv \frac{\beta}{r_m} \tag{4}$$

$U(r)$ becomes

$$U(r) = \frac{\epsilon}{\delta - \beta}\left[\beta e^{-\delta}\left(\frac{r}{r_m} - 1\right) - \delta e^{-\beta}\left(\frac{r}{r_m} - 1\right)\right] \tag{5}$$

with $U(r_m) = -\epsilon$. If we require the curvature of $U(r)$ at $r_m$ to be the same as that for $U_{LJ}$ (i.e., $72\ \epsilon/r_m^2$) and set $U(\sigma) = 0$, where $\sigma = r_m/2^{1/6}$, these two constraints yield:

$$\delta = 16.842, \quad \beta = 4.275$$

and the parameters $A$, $B$, $C$, and $D$ can be determined by eq 4.

The water$-$water interaction was represented by the MCY potential,[31] whereas cation$-$water potentials were represented by MCY parametrization of the ab initio model of Bounds.[32] Details of the validation of eq 1 and the parameters in Tables 1 and 2 for use in clay$-$water systems have been discussed in previous papers.[33$-$37] The MCY potential is strictly a pair potential and does not take account of nonpairwise additive

effects (such as induction). However, unlike empirical water potentials (TIP4P, SPC, etc.), it does not impose tetrahedral coordination. Therefore, an advantage in using the MCY potential occurs if the structure of water differs from bulk water, as it does significantly in hydrated clay systems.[33$-$37] The high quality of the MCY potential in predicting the second virial coefficient of water and detailed comparisons between it and other types of water$-$water potential, including ASP-W,[38,39] are discussed elsewhere.[40]

**2.2. Simulation Cell.** The simulation cell used was a 21.12 Å × 18.28 Å patch with two-half-layers of Wyoming-type montmorillonite, typical of bentonitic materials. This cell was replicated infinitely in three dimensions to mimic a physically observable macroscopic system. The simulation cell size (eight clay mineral unit cells) is the same as used in our earlier studies of the same clay mineral.[41,42]

The Wyoming Na-montmorillonite model used in our simulation cell has the chemical formula:[33$-$37]

$$Na_6[Si_{62}Al_2](Al_{28}Mg_4)O_{160}(OH)_{32} \tag{6}$$

Three layers of water (12 H$_2$O per unit cell in the absence of CH$_4$) were added to the simulation cell for clay hydration. This is the number of water layers observed for Na-montmorillonite equilibrated with 0.7 m NaCl,[43] the ionic strength of seawater. The precise number of interlayer water molecules varied in our simulations depending on CH$_4$ content (see below). Short-range interactions were treated with the all-image convention and a 9 Å real-space cutoff. Long-range electrostatic (Coulombic) interactions across (or beyond) the simulation cell were computed by the Ewald sum method.[44] A reciprocal space cutoff (k-space cutoff) of 2.0 Å$^{-1}$ was used for all simulations.

**2.3. Monte Carlo Simulation.** Monte Carlo (MC) simulations of montmorillonite hydrates were carried out on Cray J90 clusters at NERSC (National Energy Research Scientific Computing Center) at Lawrence Berkeley National Laboratory. A Metropolis Monte Carlo simulation code, MONTE was used.[45] Recently we have used this code to model data on adsorbed water structure based on $^1$H/$^2$D isotopic-difference neutron diffraction and X-ray reflectivity experiments performed on montmorillonite and muscovite, respectively.[33,34] All MC simulations were carried out in a constant ($N$, $\sigma$, $T$) ensemble, with absolute temperature T and the pressure applied normal to the clay layers $\sigma$ are constant.

*2.3.1. Phase Space Sampling Strategy.* The phase space sampling strategy used was as follows.[42] For the first 50 000 MC steps, only interlayer water molecules were allowed to move, while the counterions and the clay layers remained at their original positions (initial layer spacing 19 Å). For the next 50 000 MC steps, the water molecules moved and the clay layer was allowed to move only in the direction normal to its basal planes. For the next 100 000 MC steps, water molecules, Na$^+$, CH$_4$, and the clay layers were allowed to move freely, with the upper clay layer moved one step in any direction with respect to the bottom layer after every five moves of the interlayer water molecules. In the next 2 500 000 MC steps, the same conditions were applied. The last 500 000 MC steps with 1,000 realizations were used for output analysis, with data were collected every 500 steps.

*2.3.2. Initial P/T Conditions.* Initially, we imposed P/T conditions under which methane hydrates are known to be stable using the published P/T phase diagram for free methane gas in equilibration with methane hydrate.[6] We also used methane-hydrate-water equilibrium curves for seawater vs pure water.[46] A sediment depth of 500 m was used to find the corresponding

pressure and temperature from these curves. (Methane hydrates are stable at the sea-floor below 300−500 m water depth,[7,47] but are often found at much shallower depths.) The depth-to-atmospheric-pressure conversion was based on 10.1 kPa m$^{-1}$ lithostatic and hydrostatic pressure gradients[6] or a 10 MPa km$^{-1}$ hydrostatic gradient.[48] The calculated pressure for 500 m depth was 49.84 atm (1 atm = 101.325 kPa), and the corresponding temperature obtained from the P/T phase diagram[6] was approximately 5 °C. Therefore, our simulations were first initiated at 278 K and 50 atm in an (N, σ, T) ensemble.

*2.3.3. Methane Content.* We used a water/methane ratio of 5.75[49] to determine a methane loading in the interlayer region of 0.5 CH$_4$ per unit cell, taking into consideration the first solvation shell for the six Na$^+$ cations in the simulation cell, as well as the possible coordination of nonsolvation water in a methane−water clathrate. Then we systematically increased the number of methane molecules. Thus we chose 0.5, 1.0, and 2.25 CH$_4$ per unit cell and 11.5, 11.0, and 9.75 H$_2$O per unit cell for the MC simulations. Two systems (0.5 and 1.0 CH$_4$ per unit cell) have enough water molecules to hydrate all interlayer cations and methane molecules, whereas the third system (2.25 CH$_4$ per unit cell) does not have enough water molecules to support the nominal methane hydration number (water/methane ratio = 4.33 < 5.75).

*2.3.4. P/T Optimization.* The 0.5, 1.0, and 2.25 CH$_4$ per unit cell systems were phase-sampled at 10, 20, 30, 40, or 50 atm with temperature fixed at 300K. The 15 MC simulations (three systems under five different pressures) were monitored in the usual way in terms of total potential energy and layer spacing profiles. Pressures of 10, 20, and 30 atm for the 0.5, 1.0, and 2.25 CH$_4$ per unit cell systems, respectively, gave the most stable total energy and layer spacing profiles. All three systems were MC stable at pressures above these, up to 50 atm.

For optimization of temperature, we used temperatures and pressures from the P/T curve determined for hydrate synthesis in the presence of bentonite.[20] This experimental reference for P/T determinations is more reliable than pure-water phase diagrams based solely on oceanic hydrostatic pressure and temperature profiles. Using this curve, we found temperatures of 292, 294, and 295 K for pressures of 10, 20, and 30 atm, respectively. Since these temperatures are not statistically different from one another or from 300 K,[50] the simulation temperature was simply set at 300K.

*2.3.5. Three-Layer Hydrate of Na-Montmorillonite.* Monte Carlo simulation of the three-layer hydrate of Na-montmorillonite without intercalated methane was performed using the method described in sections 2.1−2.4. The simulation cell contained opposing clay mineral layers, six Na$^+$, and 12 H$_2$O per unit cell. The phase sampling strategy in section 2.3.1 was followed by a final 1 500 000 MC steps during which the water molecules, Na$^+$, and the clay layers were allowed to move freely. The last 500 000 MC steps with 1,000 realizations were used for output analysis. Data were collected every 500 steps.

**2.4. Molecular Dynamics Simulation.** Molecular dynamics (MD) simulations were carried out over 1.02 ns using the code MOLDY[51] as executed on Cray T3E clusters with the shared-memory version of the MPI message-passing library (64 processors). All MD runs were performed at NERSC.

Our simulations were initiated from coordinate feeds based on Monte Carlo simulations, where phase-space sampling was performed in an equilibrated volume (clay interlayer volume equilibrated in terms of clay layer spacing changes and shifts of the simulation cell axes) at the optimized pressures and temperature. Our microcanonical ensemble (NVE) MD simula-

tions permitted were particles in the lowest-energy MC configuration to relax while pressure and temperature were allowed to fluctuate. The bulk structure of the interlayer region then was examined to quantify the mobility of methane, sodium ions, and water molecules.[36,37]

The entire 1.02 ns molecular dynamics simulation was used to plot mean-square center-of-mass displacements (MSD),

$$\text{MSD} = \langle |r(t) - r(0)|^2 \rangle = \frac{1}{NN_t}\sum_{n=1}^{N}\sum_{t_0}^{N_t}|r_n(t+t_0) - r(t_0)|^2 \quad (7)$$

where $r_n(t)$ is the center-of-mass position of particle $n$ at time $t$, $N$ is the total number of molecules of interest, and $N_t$ is the total number of MD time steps used for statistical averaging. Self-diffusion coefficients were calculated using the Einstein relation:[44]

$$D = \frac{1}{6t}\langle |r(t) - r(0)|^2 \rangle \quad (8)$$

Velocity autocorrelation functions [$\Psi(t)$, VACF], were computed at 0.1 ps time-resolution for methane and water using the equation

$$\Psi(t) = \frac{1}{NN_t}\sum_{n=1}^{N}\sum_{t_0}^{N_t}v_n(t_0)v_n(t_0 + t) \quad (9)$$

where $v_n(t)$ is the center-of-mass velocity of particle $n$ at time $t$. We used the first 20 ps of MD results to Fourier transform the VACF to power spectra (density of states) with the highest possible resolution from our recording of the MD intermediate velocity dump. Averaging was performed over time origins $t_0$ spaced by 0.1 ps, and over all methane molecules and water molecules. The VACF was transformed into the frequency domain using a discrete Fourier transform (DFT) with a Blackman window incorporated to reduce spectral leakage (noise)[44] and obtain a smooth curve with a maximum at the correct frequency. Thus the calculated velocity autocorrelation function $\Psi(t)$ was multiplied by the Blackman window function

$$W(t) = 0.42 - 0.5 \cos\left(\frac{\pi \cdot t}{t_{max}}\right) + 0.08 \cos\left(\frac{2\pi t}{t_{max}}\right) \quad (10)$$

and the result was converted into the power spectrum $f(\omega)$:

$$f(\omega) = \sqrt{\frac{2}{\pi}}\int_0^{\infty} W(t) \cos\omega t \, dt \quad (11)$$

Spurious oscillations (side lobes) near the maxima caused by finite summation were successfully removed by using this methodology.

Radial distribution functions (RDFs) were calculated by binning site pair distances periodically throughout a simulation. The binning subroutine was invoked every 250 time steps (0.125 ps) of binning interval without losing detailed statistical information. The binning limit was set to 18 Å to include the full interlayer region and sliced into 60 binning intervals between 0 and 18 Å. Data obtained from the last 400,000 time steps (200 ps) of the 1.02 ns MD trajectories were used for RDF computations. Pair correlation functions $g(r)$ based on MD can show both equilibrium and nonequilibrium properties near
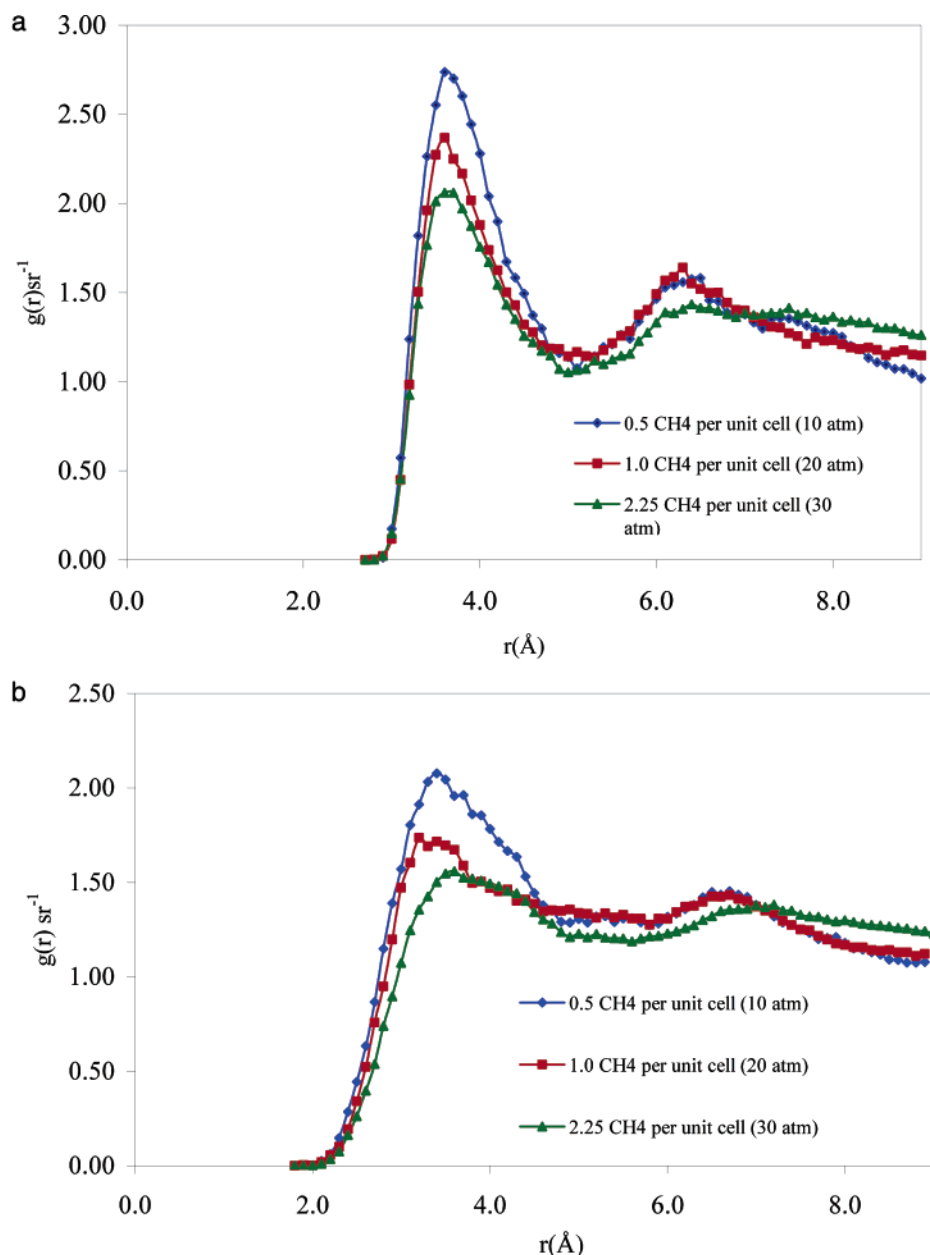
Promoting Methane Hydrate Formation

*J. Phys. Chem. B, Vol. 107, No. 10, 2003* **2285**



**Figure 1.** (a) Methane−oxygen (Me−O) radial distribution function (RDF) for 0.5, 1.0, and 2.25 CH$_4$ per unit cell systems at 300K and 10, 20, and 30 atm, respectively (2.5 million MC steps). (b) Methane−hydrogen (Me−H) radial distribution function (RDF) for 0.5, 1.0, and 2.25 CH$_4$ per unit cell systems at 300 K and 10, 20, and 30 atm, respectively (2.5 million MC steps).

equilibrium, whereas $g(r)$ based on MC can show only time-independent, equilibrium properties.[52]

**Results and Discussion**

**3.1. Methane−Water Pair Correlation.** Figure 1 shows radial distribution functions (RDFs) for Me−O and Me−H induced by methane-water spatial correlations. All three simulations showed a strong Me−O pair correlation peak near 3.7 Å, which represents the first hydration shell, in which water dipole vectors are predominantly tangential.[53] [The relative peak height in Figure 1 for the first hydration shell depends on the number of water molecules (92, 88, or 78 H$_2$O per simulation cell for 0.5, 1.0, or 2.25 CH$_4$ per unit cell) and to some extent on the pressure.] This sharp peak was followed by a broad peak near 6.2 Å (second hydration shell). An early MC simulation of the sI hydrate[54] yielded Me−O distances from 3.2 to 5.7 Å, with a peak at 4.1 Å, and MC simulation of dilute methane solution gave a broad first hydration shell at 3.1 to 6.0 Å.[55]

Me-O coordination numbers were calculated with the RDFs in Figure 1. The running coordination number $n(r)$ was computed by integration up to the first minimum after the first Me-O correlation peak. At $r = 5.5$ Å, coordination numbers of 20−22 for both 0.5 and 1.0 CH$_4$ per unit cell were calculated. The MC simulations of Titiloye and Skipper[28] using the empirical TIP4P model for two layers of water within the clay interlayer also showed a Me−O correlation peak near 5.5 Å with a coordination number of 19. Our Me−O coordination number of 20−22 for three layers of water is consistent with previous simulations of isolated methane clathrates in bulk liquid water at 298.15 K using the MCY potential[56] and of the structure of the sI hydrate at 145 K using the SPC potential.[54]

Koh et al.[25] used neutron diffraction with H/D isotopic substitution to investigate changes in local water structure around methane during hydrate formation. They determined methane−water (carbon−oxygen) pair correlation functions to characterize the structure of the hydration shell, reporting a methane
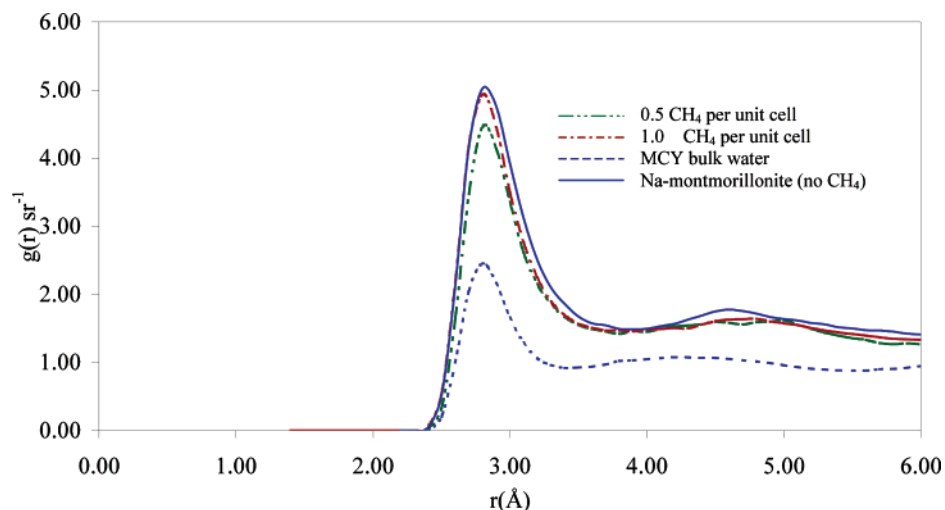
**2286** *J. Phys. Chem. B, Vol. 107, No. 10, 2003*

Park and Sposito



**Figure 2.** Oxygen−oxygen pair correlation of interlayer water (O−O RDF) for 0.5 and 1.0 CH₄ per unit cell systems (compared with MCY bulk liquid water).
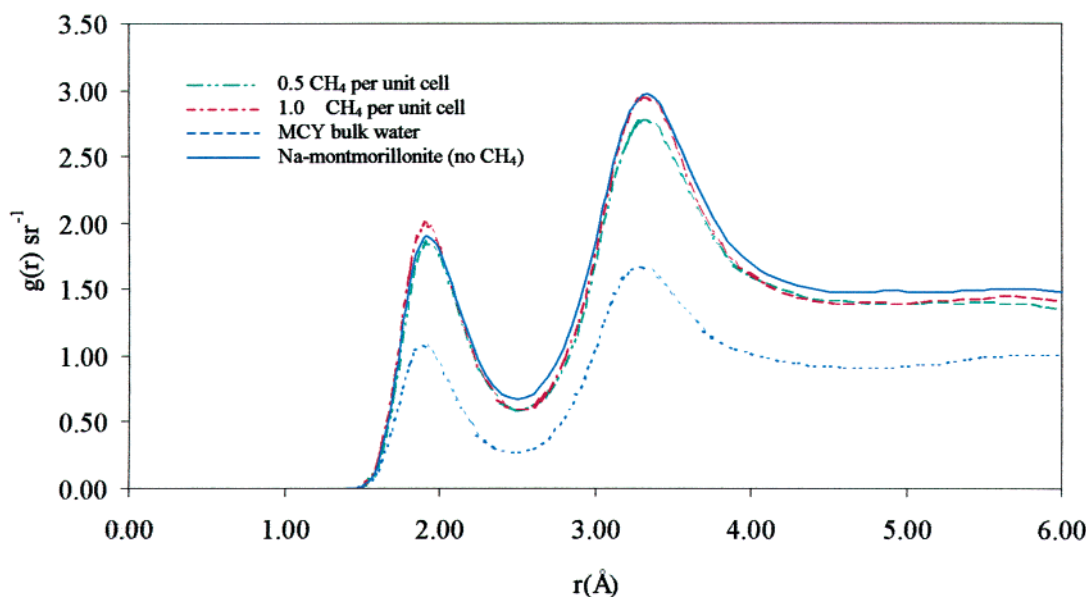


**Figure 3.** Oxygen−hydrogen pair correlation of interlayer water (O−H RDF) for 0.5 and 1.0 CH₄ per unit cell systems (compared with MCY bulk liquid water).

coordination number around $16 \pm 1$ during hydrate formation, whereas the fully formed stable hydrate had a coordination number of $21 \pm 1$. The coordination numbers from two of our MC simulations are in good agreement with this latter Me−O coordination number. Furthermore, the overall Me−O pair correlation profile and peak locations determined by Koh et al.[25] are strikingly similar to our results for the 0.5 and 1.0 CH₄ per unit cell systems. A Me−O coordination number of only 16 was obtained for the 2.25 CH₄ per unit cell system in our MC simulation. Therefore, on the basis of previous experimental and simulation results, we conclude that the 2.25 CH₄ per unit cell system did not form a typical methane hydrate.

**3.2. Interlayer Water Structure.** The organization of water in the clay interlayer region is depicted by O−O and O−H RDFs in Figures 2 and 3, respectively. Corresponding nearest-neighbor O−H and O−O coordination numbers are listed in Table 3. The structure of water in the three-layer hydrate differs from that of bulk liquid water.[57] The O−O pair correlation in clay interlayer water extends further with or without CH₄ (up to 3.9 Å), and the interlayer methane clathrate systems have O−O coordination numbers of 5.54 and 5.55, which are greater than

**TABLE 3: Intermolecular Coordination Values for O−O, O−H for 0.5 and 1.0 CH₄ per Unit Cell Systems Compared with Those for Interlayer and Bulk Liquid Water**

| $N_{OO}$ | $r_{min}$ (Å) | $N_{OH}$ | $r_{min}$ (Å) |
|---|---|---|---|
| | Liquid Water[a] | | |
| 5.40 | 3.5 | 1.02 | 2.5 |
| | Three-Layer Hydrate of Na-Montmorillonite (18.77 Å)[b] | | |
| 4.90 | 3.9 | 1.62 | 2.4 |
| | 0.5 CH₄ per Unit Cell/Na-Montmorillonite (18.53 Å)[b] | | |
| 5.54 | 3.8 | 1.61 | 2.5 |
| | 1.0 CH₄ per Unit Cell/Na-Montmorillonite (19.40 Å)[b] | | |
| 5.55 | 3.8 | 1.58 | 2.5 |

[a] From refs 33 and 42. [b] Layer spacing (clay mineral + interlayer).

for both liquid water and Na-montmorillonite without CH₄. This increase in O−O coordination in interlayer methane clathrate sytems is likely due to the combined disruptive effects of clathrate formation around methane (hydrophobic effect), solvation of Na⁺, and hydration of the clay mineral surface. The O−H coordination numbers of the interlayer methane clathrates are greater than for liquid water but similar to Na-montmoril-
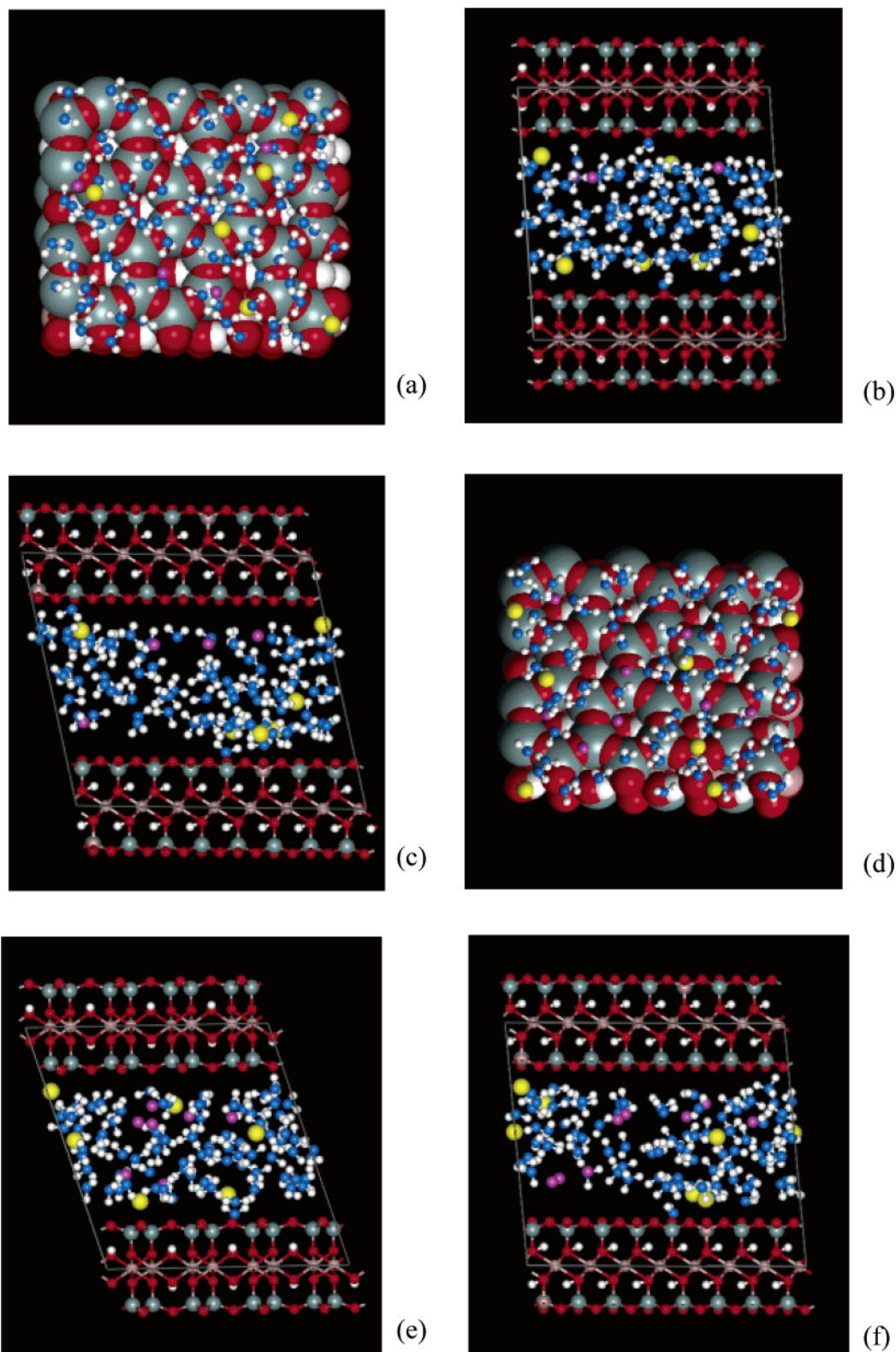
Promoting Methane Hydrate Formation

*J. Phys. Chem. B, Vol. 107, No. 10, 2003* **2287**



**Figure 4.** MC snapshot for the 0.5 CH$_4$ and 1.0 CH$_4$ per unit cell systems. Water molecules and counterions are shown together with methane and the clay mineral structure. The red spheres represent mineral O, the gray spheres represent mineral Si, and the pink spheres represent Al in tetrahedral charge substitution sites in place of Si and Al in octahedral layer. Water O are blue and H are white, while Na are yellow and methane molecules are purple; MC snapshot for the 0.5 CH$_4$ per unit cell system: (a) top view (*ab* plane; upper clay structure removed), (b) side view (*bc* plane), (c) side view (*ac* plane); MC snapshot for 1.0 CH$_4$ per unit cell system: (e) top view (*ab* plane), (f) side view (*bc* plane), (g) side view (*ac* plane).

lonite interlayer water without CH$_4$. Therefore, the interlayer water in the presence of methane clathrate has a highly disrupted hydrogen bonding network as compared to bulk liquid water.

**3.3. MC Snapshots of Clathrate Structure.** Figure 4 visualizes the equilibrium structure in the 0.5 CH$_4$ per unit cell

and 1.0 CH$_4$ per unit cell systems. (Detailed information about our MC results using three-dimensional visualization with fast rendering is available electronically.[58]) Methane molecules (purple) are seen to be well dispersed within the clay interlayer, while water molecules (blue O) and hydrated Na$^+$ ions (yellow)
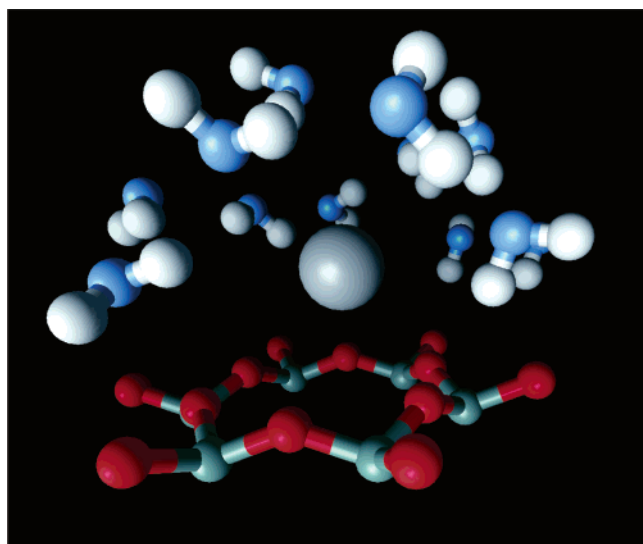
**Figure 5.** Closeup snapshot of methane clathrate near a clay mineral surface. The methane-22 oxygen coordination observed involves both methane−water and methane−clay surface interactions. The methane molecule (gray) is surmounted by an umbrella-like water (blue O) structure, while below it is a hexagonal ring of clay surface oxygens.

surround them. The methane hydrate sI structure has two types of clathrate structures having pentagons ($5^{12}$) or pentagons and hexagons ($5^{12} 6^2$). Unlike these ideal methane hydrate clathrates, where only water molecules are present, Figure 4 shows the methane molecules to be found near the clay mineral oxygen surface. Most of the water molecules reside at the midplane of the simulation cell where they can form a cage around a methane molecule while distancing themselves from the clay mineral surface. Figure 5 shows the local organization of a methane clathrate in the 0.5 $CH_4$ per unit cell system. The methane molecule is surmounted by an a clathrate-like water structure, while below it is a hexagonal ring of clay surface oxygens. The overall methane-22 oxygen coordination is thus shared between both water and clay oxygens. Clathrate water molecules are found aligned in two principal layers above a ditrigonal cavity in the clay mineral surface. This 22 $CH_4$−O clathrate structure is thus a distorted form of either the pentagonal dodecahedron ($5^{12}$) or tetrakidecahedron ($5^{12}6^2$) in the ideal methane hydrate. We propose that this disordered clathrate structure can occur in smectitic sediments bearing methane hydrates, with a portion of the clay surface actively involved in promoting clathrate formation. The constraints of restricted interlayer space, cation solvation, and disrupted water network near the clay surface are important to an enhanced clathrate formation. Most significantly, there is structural synergism between the hexagonal array of clay surface oxygens and hydrogen-bonded water molecules.

**3.4. Diffusion of Interlayer Components.** A routine method of least squares was applied to obtain slopes of the MSD vs time curves. Self-diffusion coefficients calculated using eq 8 are tabulated in Table 4 along with related experimental data and simulation results. The self-diffusion coefficient of the water molecule differed from that in bulk water[59] in all three methane hydrate simulations. Slower diffusion of interlayer water as compared to bulk water was also found in hydrated Na-montmorillonite without methane intercalation.[37] The diffusion coefficient of methane was lower than that of water only in the 0.5 $CH_4$ per unit cell system, in which it was also lower than that of methane in bulk liquid water. Therefore, the MSDs and self-diffusion coefficients suggest that only the 0.5 $CH_4$ per unit cell system contains a dynamically stable methane clathrate.

**TABLE 4: Self-Diffusion Coefficients ($10^{-9}$ m$^2$ s$^{-1}$) Computed from the Mean Square Center-of-Mass Displacement Using the Einstein Relation (Equation 8)**

| system | methane | water | Na$^+$ |
|---|---|---|---|
| Na-montmorillonite three-layer hydrate[a] | | 0.72 | 0.11 |
| 0.5 $CH_4$ per unit cell | 1.135 | 1.955 | 0.14 |
| 1.0 $CH_4$ per unit cell | 2.319 | 1.676 | 0.13 |
| bulk liquid water | 1.49[b] | 2.3[c] | 0.20[d] |

[a] MD simulation (205 ps) at 300 K based on the MCY model for the three layer-hydrate of Na-montmorillonite.[37]  [b] Experimental result, 298 K.[29]  [c] Experimental result, 298 K.[59]  [d] Experimental result, 298 K.[69]

**3.5. Velocity Autocorrelation Function and Power Spectrum.** The VACF for water in the 0.5, 1.0, and 2.25 $CH_4$ per unit cell systems exhibited minimal differences from one another in terms of an initial quick decay and subsequent oscillation about zero (data not shown). However, the VACF for methane showed differences at different methane loadings (data not shown). Sharpness in the methane VACF oscillation has been attributed to formation of the clathrate structure.[60] Both the 0.5 and 1.0 $CH_4$ per unit cell systems showed sharp oscillations after quick decay over a 0.2−0.3 ps time domain. However, the VACF of the 0.5 $CH_4$ per unit cell system exhibited sharper peaks with greater amplitude fluctuations, although most of the maxima and minima of the oscillation occurred at points of the time domain very similar to those for the 1.0 $CH_4$ per unit cell system. Power spectra for methane based on the VACFs are presented in Figure 6, while peak frequencies in the power spectra are listed in Table 5. Experimental[61,62] and theoretical (MD)[26,54,63−68] values of characteristic wavenumbers for methane hydrate power spectra are also compiled in the table. All previous MD results and experimental data contain peaks near 50 and 90 cm$^{-1}$. Neutron scattering data[61,62] show a 110 cm$^{-1}$ peak, which was also found in the present study. Indeed, all of the peaks found for the 0.5 $CH_4$ per unit cell system occur as well in published power spectra based on neutron scattering data. Therefore, this system shows the same characteristic power spectrum as found for methane hydrates in pure water.

In methane hydrate MD simulations at varying temperature,[62] splitting and broadening of the peaks in the power spectrum have been associated with increased temperature. This makes the hydrate structure metastable against collapse into bulk phases (water + gas). In our simulations, a similar kind of splitting and broadening of the peaks in the power spectrum was observed for the systems at higher interlayer methane concentrations (1.0 and 2.25 $CH_4$ per unit cell). The sharp peaks with little splitting found in the 0.5 $CH_4$ per unit cell system thus represent a stable methane hydrate. Evidently increasing the methane interlayer concentration has an effect on methane hydrate stability similar to increasing temperature.

The presence of mode coupling between guest and host molecules can be evaluated by comparing the power spectrum of the guest (methane) molecule to that of the host (water) molecule in the wavenumber region ≤160 cm$^{-1}$ (Figure 6). The $H_2O$ power spectrum (not shown) did not indicate significant differences at different loadings of methane molecules, whereas the $CH_4$ power spectrum for the 0.5 $CH_4$ per unit cell system showed major differences in the density of states at ∼13, 60, and ∼110 cm$^{-1}$ as compared to the 1.0 $CH_4$ system (Figure 6) and the 2.25 $CH_4$ per unit cell system (data not shown). Therefore, no indication of mode coupling was found. Rodger[26] has discussed correlation between host dynamics and guest dynamics as an indication of mode coupling in methane hydrate stabilization, concluding that, if the characteristic frequencies
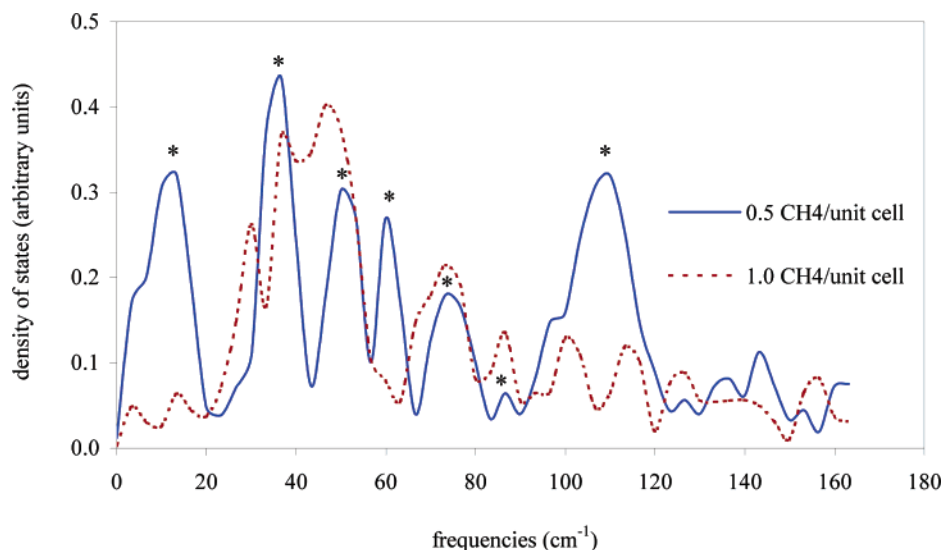
Promoting Methane Hydrate Formation

*J. Phys. Chem. B, Vol. 107, No. 10, 2003* **2289**



**Figure 6.** Simulated power spectra of methane translational motions for the 0.5 and 1.0 CH$_4$ per unit cell systems. The asterisks (*) correspond to experimentally measured methane clathrate frequencies.

**TABLE 5: Characteristic Wavenumbers (in cm$^{-1}$) for Translational Motions of Methane and Water Molecules**

| author | description of the study | characteristic wavenumbers |
|---|---|---|
| this work | MD (300 K) 0.5 CH$_4$/unit cell in hydrated Na-montmorillonite, | 13, 37, 50, 60, 73, [87],[a] 110 |
| | MD (300 K) 1.0 CH$_4$/unit cell in hydrated Na-montmorillonite, | [3], [13], 30, 37, 47, 73, [87, 100, 113] |
| Forrisdahl et al.[63] | MD (270 K) 5.75 water/CH$_4$ in solid hydrate | 50, 72, 89 |
| Tse et al.[62] | IINS experimental (5 K) deuterated sI methane hydrate | 13, 36, 50, 60, 73, 86, 100, 109, 113 |
| Rodger[66] | MD (270 K) 5.75 water /CH$_4$ in solid hydrate | 91, 99 |
| Tanaka and Kiyohara[68] | MD (273 K) 5.75 water /CH$_4$ in solid hydrate | 50, 90 |

[a] Weak peak in "[ ]".

of translation of the guest molecule are similar to those of host lattice vibrations, there can be mode coupling between the two motions which would lower the energy of the clathrate, hence increase its stability. For the interlayer hydrate, however, if the dynamics of the methane molecule have an important role in the stabilization of the clathrate, it is not in the form of dynamic coupling with the host. This suggests that we can interpret the dynamics of interlayers methane hydrates using solely the concept of guest−host interactions.[26]

**3.6. Dynamic Methane−Water Pair Correlation.** The simulations of the 0.5 and 1.0 CH$_4$ per unit cell systems showed a Me-O peak at ∼3.75 Å in the MD pair correlation function. This peak also was observed in our MC RDFs and attributed to the first hydration shell of methane. Detailed consideration of the MD Me-O pair correlations in the 0.5 and 1.0 CH$_4$ per unit cell systems provides insight similar to that obtained from MSDs and self-diffusion coefficients, on the basis of which we concluded that only the 0.5 CH$_4$ per unit cell system shows true clathrate formation. A small negative shift (0.5 Å, to smaller r) of the first minimum in the Me-O pair correlation function was observed for the 1.0 CH$_4$ per unit cell system relative to the 0.5 CH$_4$ per unit cell system. Recent neutron diffraction data have confirmed that the water shell around methane in the crystalline hydrate is significantly larger than the shell formed in bulk water.[25] Therefore, the 1.0 CH$_4$ per unit cell system may represent a methane hydrate somewhat like that observed in dilute solution.

## 4. Conclusions

We have examined by molecular simulation the hypothesis of a "thermodynamic promotion effect" for a 2:1 clay mineral surface based on experimental observation of the dissociation of methane hydrate at higher temperature (∼295 K) and lower

pressure (30−50 atm) in the presence of bentonite than for the same process in water alone.[20−22] The 0.5 and 1.0 CH$_4$ per unit cell systems we investigated showed 20−22 Me−O nearest-neighbor coordination (at r = 5.5 Å), whereas the 2.25 CH$_4$ per unit cell system showed only 16 Me−O coordination. In the 0.5 CH$_4$ per unit cell system, the methane molecule is surrounded by a stable clathrate-like water structure and rests adjacent to the hexagonal array of clay surface oxygens (Figure 5). Disruption of the normal tetrahedral network of bulk water in the 0.5 and 1.0 CH$_4$ per unit cell systems is attributed to the combined effects of the clay mineral surface, counterions, and methane clathrate formation. Our MD simulations confirmed that the 2.25 CH$_4$ per unit cell system was not a stable hydrate. The 1.0 CH$_4$ per unit cell system was also deemed unstable by MD simulation because of the relatively high self-diffusion coefficient of methane and contracted size of the water clathrate (shift in the Me−O pair correlation function). In the power spectra (Figure 6), we found the same peaks for 0.5 CH$_4$ per unit cell system as in experimental and theoretical spectra for methane hydrate in pure water. The power spectrum of 1.0 CH$_4$ per unit cell system included 3, 30, and 47 cm$^{-1}$ peaks which were not characteristic wavenumbers according to the tabulated experimental and simulation results. On the other hand, it also lacked the characteristic hydrate peaks at 50, 60, and 110 cm$^{-1}$. The possibility of a mode-coupling effect as a stabilizing mechanism for the interlayer methane hydrate was eliminated in favor of the host−guest interaction mechanism. On the basis of these MC and MD simulations, a new structure for natural methane hydrate is proposed in which a portion of a 2:1 clay mineral surface is actively involved in promoting clathrate formation.

## References and Notes

(1) Sloan, E. D., Jr. Physical/Chemical Properties of Gas Hydrates and Application to World Margine Stability and Climate Change. In *Gas Hydrates: Relevance to World Margin Stability and Climate Change*; Henriet, J.-P., Mienert, J., Eds.; Special Publications ed; Geological Society: London, 1998; Vol. 137; pp 31−50.

(2) Englezos, P. *Ind. Eng. Chem. Res.* **1993**, *32*, 1251−1274.

(3) van der Waals, J. H.; Platteeuw, J. C. *Adv. Chem. Phys.* **1959**, *2*, 1−57.

(4) Buffett, B. A. *Annu. Rev. Earth Planet. Sci.* **2000**, *28*, 477−507.

(5) Dillon, W. P.; Lee, M. W.; Coleman, D. F. *Ann. N. Y. Acad. Sci.* **1994**, *715*, 364−380.

(6) Kvenvolden, K. A. *Rev. Geophys.* **1993**, *31*, 173−187.

(7) Kvenvolden, K. A. *Proc. Natl. Acad. Sci. U.S.A.* **1999**, *96*, 3420−3426.

(8) Haq, B. U. *Science* **1999**, *285*, 543−544.

(9) Sparks, K. A.; Tester, J. W. *J. Phys. Chem.* **1992**, *96*, 11022−11029.

(10) Hyndman, R. D.; Davis, E. D. *J. Geophys. Res.* **1992**, *97*, 7025−7041.

(11) Paull, C. D.; Ussler, W.; Borowski, W. S. *Ann. N. Y. Acad. Sci.* **1994**, *715*, 392−409.

(12) Xu, W.; Ruppel, C. *J. Geophys. Res.* **1999**, *104*, 5081−5095.

(13) Rempel, A. W.; Buffett, B. A. *J. Geophys. Res.* **1997**, *102*, 10151−10164.

(14) Grim, R. E.; Guven, N. *Bentonites: Geology, Mineralogy, and Uses*; Elsevier: New York, 1978.

(15) Kastner, M. *Proc. Natl. Acad. Sci. U.S.A.* **1999**, *96*, 3380−3387.

(16) Clennell, M. B.; Hovland, M.; Booth, J. S.; Henry, P.; Winters, W. J. *J. Geophys. Res.−Solid Earth* **1999**, *104*, 22985−23003.

(17) Balsam, W. L.; Damuth, J. E. Further Investigations of Shipboard vs Shore-Based Spectral Data: Implications for Interpreting Leg 164 Sediment Composition. *Proc. ODP, Sci. Results*, College Station, TX. **2000**, *164*.

(18) Collett, T. S.; Wendlandt, R. F. Formation Evaluation of Gas Hydrate-Bearing Marine Sediments on the Blake Ridge with Downhole Geochemical Log Measurements. *Proc. ODP, Sci. Results*, College Station, TX. **2000**, *164*.

(19) Güven, N. *Rev. Mineral.* **1989**, *19*, 497−559.

(20) Cha, S. B.; Ouar, H.; Wildeman, T. R.; Sloan, E. D. *J. Phys. Chem.* **1988**, *92*, 6492−6494.

(21) Ouar, H.; Cha, S. B.; Wildeman, T. R.; Sloan, E. D. *Chem. Eng. Res. Des.* **1992**, *70*, 48−54.

(22) Kotkoskie, T. S.; Al-Ubaldi, B.; Wildeman, T. R.; Sloan, E. D., Jr. *SPE Drill. Eng.* **1992**, 130−136.

(23) Mitchell, J. K. *Fundamentals of Soil Behavior*, 2nd ed.; John Wiley: New York, 1993.

(24) Buffett, B. A.; Zatsepina, O. Y. *Mar. Geol.* **2000**, *164*, 69−77.

(25) Koh, C. A.; Wisbey, R. P.; Wu, X.; Westacott, R. E.; Soper, A. K. *J. Chem. Phys.* **2000**, *113*, 6390−6397.

(26) Rodger, P. M. *Mol. Simulat.* **1990**, *5*, 315−328.

(27) Rodger, P. M. *J. Phys. Chem.* **1990**, *94*, 6080−6089.

(28) Titiloye, J. O.; Skipper, N. T. *Chem. Phys. Lett.* **2000**, *329*, 23−28.

(29) Lide, D. R. *Handbook of Chemistry and Physics*, 79th ed.; CRC Press: Boca Raton, FL, 1998.

(30) Skipper, N. T.; Bridgeman, C. H.; Buckingham, A. D.; Mancera, R. L. *Faraday Discuss.* **1996**, *103*, 141−150.

(31) Matsuoka, O.; Clementi, E.; Yoshimine, M. *J. Chem. Phys.* **1976**, *64*, 1351−1361.

(32) Bounds, D. G. *Mol. Phys.* **1985**, *54*, 1334−1355.

(33) Park, S.-H.; Sposito, G. *J. Phys. Chem. B* **2000**, *104*, 4642−4648.

(34) Park, S.-H. and Sposito, G. *Phys. Rev. Lett.* **2002**, *89*, 85501.

(35) Skipper, N. T.; Chang, F.-R. C.; Sposito, G. *Clays Clay Miner.* **1995**, *43*, 285−293.

(36) Chang, F.-R. C.; Skipper, N. T.; Sposito, G. *Langmuir* **1998**, *14*, 1201−1207.

(37) Chang, F.-R. C.; Skipper, N. T.; Sposito, G. *Langmuir* **1997**, *13*, 2074−2082.

(38) Millot, C.; Soetens, J.-C.; Martins Costa, M. T. C.; Hodges, M. P.; Stone, A. J. *J. Phys. Chem. A* **1998**, *102*, 754−770.

(39) Leforestier, C.; Braly, L. B.; Liu, K.; Elrod, M. J.; Saykally, R. J. *J. Chem. Phys.* **1997**, *106*, 8527.

(40) Park, S.-H. *MCY vs ASP−W Potential Surface of Water Dimer*; Earth Sciences Division, Lawrence Berkeley National Laboratory: Berkeley, CA, 1999.

(41) Chang, F.-R. C.; Skipper, N. T.; Sposito, G. *Langmuir* **1995**, *11*, 2734−2741.

(42) Sposito, G.; Park, S.-H.; Sutton, R. *Clays Clay Miner.* **1999**, *47*, 192−200.

(43) Posner, A. M.; Quirk, J. P. *J. Colloid Sci.* **1964**, *19*, 798−812.

(44) Allen, M. P.; Tildesley, D. J. *Computer Simulations of Liquids*; Oxford University Press: Oxford, UK, 1987.

(45) Skipper, N. T. *MONTE User's Manual*; Department of Physics and Astronomy, University College: London, 2000.

(46) Dickens, G. R.; Quinby-Hunt, M. S. *J. Geophys. Res.* **1997**, *102*, 773−783.

(47) Kukowski, N.; Pecher, I. A. *Mar. Geol.* **2000**, *164*, 1.

(48) Henry, P.; Thomas, M.; Clennell, M. B. *J. Geophys. Res.−Solid Earth* **1999**, *104*, 23005−23022.

(49) Kvenvolden, K. A. *Org. Geochem.* **1995**, *23*, 997−1008.

(50) To check this point, one must do a linear regression of $1/T$ vs ln P and see how large is the standard error of estimate. Estimated temperatures with 95% confidence limit are 285.6−312.0, 286.2−317.6, and 286.5−320.9 K, for 10, 20, and 30 atm, respectively.

(51) Refson, K. *Comput. Phys. Commun.* **2000**, *126*, 309−328.

(52) Frenkel, D.; Smit, B. *Understanding Molecular Simulation: From Algorithms to Applications*; Academic Press: San Diego, 1996.

(53) Skipper, N. T. *Chem. Phys. Lett.* **1993**, *207*, 424−428.

(54) Tse, J. S.; Klein, M. L.; McDonald, I. R. *J. Phys. Chem.* **1983**, *87*, 4198−4203.

(55) Owicki, J. C.; Scheraga, H. A. *J. Am. Chem. Soc.* **1977**, *99*, 7413−7418.

(56) Swaminathan, S.; Harrison, S. W.; Beveridge, D. L. *J. Am. Chem. Soc.* **1978**, *100*, 5705−5712.

(57) Soper, A. K.; Bruni, F.; Ricci, M. A. *J. Chem. Phys.* **1997**, *106*, 247−254.

(58) Park, S.-H. *Molecular Simulations of Hydrated Montmorillonite Interlayers*; Lawrence Berkeley National Laboratory: Berkeley, CA, 2000 (http://esd.lbl.gov/GEO/aqueous_geochem/index.html).

(59) Sposito, G. *J. Chem. Phys.* **1981**, *74*, 6943.

(60) Fujii, K.; Arata, Y.; Tanaka, H.; Nakahara, M. *J. Phys. Chem. A* **1998**, *102*, 2635−2640.

(61) Tse, J. S. Dynamical Properties and Stability of Clathrate Hydrates. In *First International Conference on Natural Gas Hydrates*; Sloan, E., Happel, J., Hnatow, M., Eds.; New York Academy of Sciences: 1994; Vol. 715, pp 187−206.

(62) Tse, J. S.; Ratcliffe, C. I.; Powell, B. M.; Sears, V. F.; Handa, Y. P. *J. Phys. Chem. A* **1997**, *101*, 4491−4495.

(63) Forrisdahl, O. K.; Kvamme, B.; Haymet, A. D. J. *Mol. Phys.* **1996**, *89*, 819−834.

(64) Plummer, P. L. M.; Chen, T. S. *J. Phys. Chem.* **1983**, *87*, 4190−4197.

(65) Tse, J. S.; Klein, M. L.; McDonald, I. R. *J. Chem. Phys.* **1984**, *81*, 6146−6153.

(66) Rodger, P. M. *J. Phys. Chem.* **1989**, *93*, 6850−6855.

(67) Tanaka, H.; Kiyohara, K. *J. Chem. Phys.* **1993**, *98*, 4098−4109.

(68) Tanaka, H.; Kiyohara, K. *J. Chem. Phys.* **1993**, *98*, 8110−8118.

(69) Nye, P. H. *Adv. Agron.* **1979**, *31*, 225.